View metadata, citation and similar papers at core.ac.uk
brought to you by CORE
provided by NASA Technical Reports Server

Spectrometer Scan Mechanism for Encountering Jovian Orbit Trojan Asteroids

Kenneth A. Blumenstock*, Alexander K. Cramer*, Joseph C. Church*, Jason A. Niemeyer*,
Fil A. Parong*, Sam Zhao*, Nerses V. Armani**, and Kenneth Y. Lee**

Abstract

This paper describes the design, testing, and lessons learned during the development of the Lucy Ralph (L'Ralph) Scan Mirror System (SMS), composed of the Scan Mirror Mechanism (SMM), Differential Position Sensor System (DPSS) and Mechanism Control Electronics (MCE). The L'Ralph SMS evolved from the Advanced Topographic Laser Altimeter System (ATLAS) Beam Steering Mechanism (BSM), so design comparisons will be made. Lucy is scheduled to launch in October 2021, embarking upon a 12-year mission to make close range encounters in 2025 and 2033 with seven Trojan asteroids and one main belt asteroid that are within the Jovian orbit. The L'Ralph instrument is based upon the New Horizons Ralph instrument, which is a panchromatic and color visible imager and infrared spectroscopic mapper that slewed the spacecraft for imaging. The L'Ralph SMM is to provide scanning for imaging to eliminate the need to slew the spacecraft. One purpose of this paper is to gain understanding of the reasoning behind some of the design features as compared with the ATLAS BSM. We will identify similarities and differences between the ATLAS BSM and the L'Ralph SMM that resulted from the latter's unique requirements. Another purpose of this paper is to focus upon "Lessons Learned" that came about during the development of the L'Ralph SMM and its MCE, both mechanism engineering issues and solutions as well as Ground Support Equipment (GSE) issues and solutions that came about during the validation of requirements process. At the time of this writing, the L'Ralph SMM has been flight qualified and delivered to the project.

Evolution of the L'Ralph Scan Mirror Mechanism (SMM)

Let us consider the ATLAS Beam Steering Mechanism (BSM) depicted in Figure 1 as our basis of comparision.[1] The ATLAS BSM's purpose is to point rather than to scan. It has two degrees of freedom provided by a custom flexure design, locating orthogonal axes of rotation behind a relatively heavy glass mirror with a dielectric coating. With the flexure axes location well behind the mirror, the actuators provide some counterbalancing, but the tungsten counterweight attached by its titanium shaft is the predominant means for balancing. Four custom voice coil actuators with redundant windings provide two axis actuation and damping. A non-redundant inductive sensing system with two axes incorporates two pairs of differential sensors which view aluminum target areas at four locations of the moving plate behind the mirror. The angular range of each axis is +/- 5 milliradians (mRad). On-orbit operating temperature is 10° C to 35° C.

The L'Ralph SMM depicted in Figure 2 requires only a single axis of rotation with an angular range of +/- 36 mRad, more than seven times the BSM angular range. The mirror is lightweighted aluminum rather than glass with the sensor targets incorporated into the backside of the mirror. The inductive displacement sensor technology has a full range linear displacement resolution compatible with both BSM and SMM, though in terms of angular resolution, BSM and SMM are quite different since their angular ranges are quite different. Due to SMM required redundancy, two sensor pairs were moved as close together as the target diameters would allow. This achieved the needed angular range and resolution, such that the inductive sensor pairs operated over their full linear displacement range of +/- 0.25 mm. With a single axis system, it was convenient and beneficial to locate conventional flex-pivots on a rotation axis that passes through the mirror. This allowed locating the axis such that mass was balanced without the need for a shaft and counterweight, saving significant mass and eliminating additional structural dynamics.

* NASA Goddard Space Flight Center (GSFC), Greenbelt, MD
** ATA Aerospace, LLC, Greenbelt, MD

Proceedings of the 45th Aerospace Mechanisms Symposium, NASA Johnson Space Center, May 13-15, 2020

The flex-pivots selected were typical brazed type rather than the higher strength electron-beam welded type. Electron-beam welded type flex-pivot fatigue life is recommended to be derated according to a technical note by Donegan, Richard J., "Weld versus Braze," (n.d.) at the Riverhawk Co., Inc. website.[2]

It has become a common practice of the GSFC Electro-Mechanical Systems branch to incorporate significant damping into actuators of precision pointing and scanning mechanisms as a means to reduce the effect of both external and internal disturbances, reducing controller burden, thus improving success in meeting performance requirements. In linear actuators, this is accomplished by a pair of connected copper sleeves that surround both the OD and ID of the bobbin. Often, it would be desired to have even higher damping than we incorporate, but it can become impractical due to actuator size limitations. Scan rates must be low enough to incorporate high damping such that actuator power to overcome damping is not significant. For the SMM, the actuator is a stretched version of the BSM actuator in order to meet SMM stroke needs, but damping is roughly doubled due to a much lower on-orbit operational temperature range of -120°C to -89°C, which reduces resistance thus increasing damping. At the low temperature extreme, the system is nearly critically damped.

The SMM Mechanism Control Electronics (MCE) incorporates a Field-Programmable Gate Array (FPGA). The Jovian orbit puts the spacecraft rather far from the sun, reducing solar array effectiveness. This resulted in the imposition of a power requirement for the MCE of less than 4 watts, significantly lower than the BSM MCE which required 13 watts. Fortunately, the sensor system is a relatively low power device requiring 0.4 watts. The BSM MCE utilized high resolution ADCs with low-noise op amps for the feedback signal. Identical components were unnecessarily used in greater quantities for telemetry, along with multiplexers, all of which are rather power hungry components. For the SMM MCE, significantly reducing the number of telemetry signals, implementing standard noise op amps, and lower resolution ADCs with built in multiplexing, reduced power considerably. For the controller feedback signals, the heritage components were kept to maintain optimal closed-loop performance. Power savings also resulted from the reduction in components since only single-axis control was needed. Substituting a low quiescent power amplifier for driving the actuator pair saved an additional 0.5 watts over the previously used power op-amp.

Scan Mirror Optical Challenges

The primary challenge of the Scan Mirror design depicted in Figure 3 was to satisfy the flatness requirement of the optical surface, 45 nanometers RMS, while balancing size and inertia. In order to minimize thermal distortion effects, the primary material for the structure of the Telescope Assembly, including all mirrors, was selected to be aluminum 6061-T651. All components which contribute to the system alignment were thermal cycled during the fabrication process to provide dimensional stability in the operating temperature environment. The optical surfaces were diamond turned and then silver coated for optimal reflectance in the specified wavelength range. The Scan Mirror geometry was selected to minimize flatness impacts from gravity release, diamond turning "fling," assembly, and on-orbit thermal gradient effects. Pocketing and tapering of the mirror was used to reduce mass while maintaining stiffness. All of these sensitivities were predicted and the design guided by finite element and other analysis tools. The Scan Mirror also had to possess features for mechanical interface, alignment references and fiducials, as well as conductive targets within the back of the mirror for the inductive displacement sensors.

The Scan Mirror is supported by three aluminum blade-style flexures to provide a secure and reliable load path that is tolerant to mounting process imperfections and thermal gradients. Alloy 7075-T651 was selected to provide the strength necessary to survive launch loads without the coefficient of linear thermal expansion (CTE) change that would be necessary with a more traditional titanium or other alternative material flexure. The flexures feature clearances at pin locations to absorb manufacturing tolerances. The flexures are bolted to the mirror and moving housing with accompanying plates that possess cavities which, during assembly, are injected with epoxy to register the flexure position to the pins. Figure 4 depicts a flexure as well as an accompanying plate configured for this process, known as "liquid pinning."

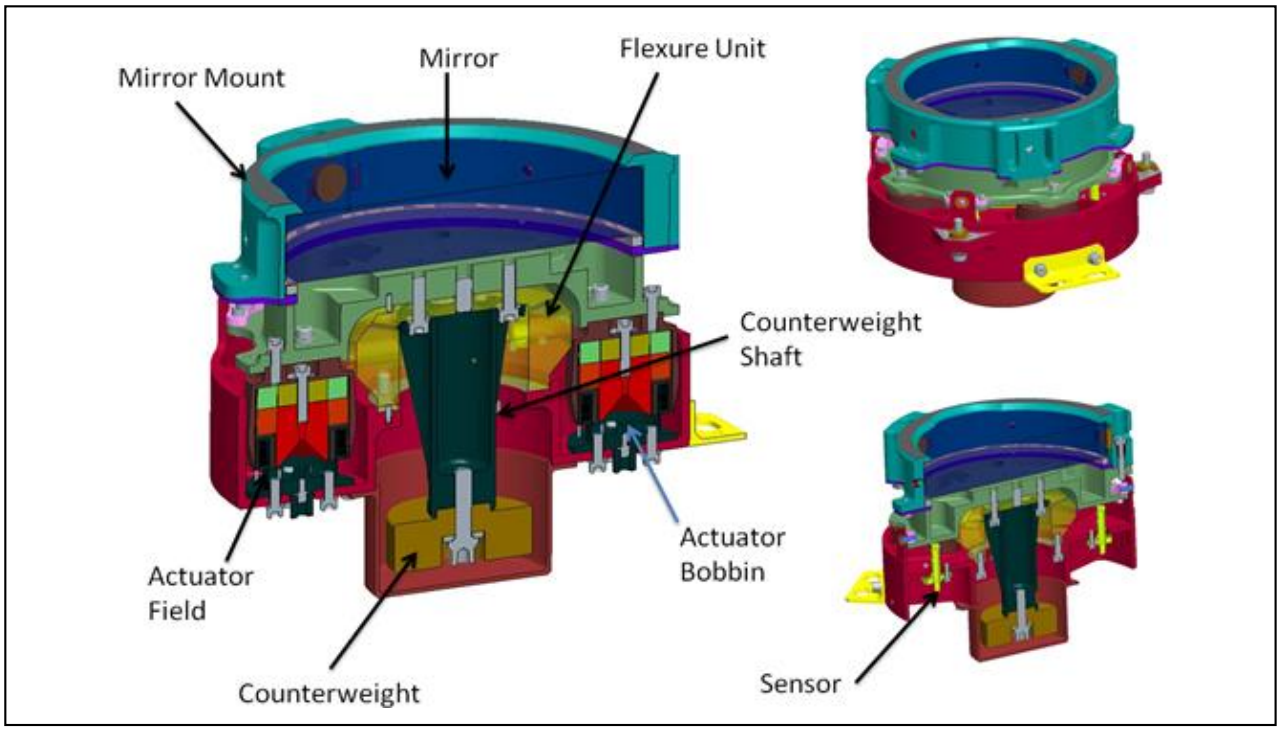

Figure 1 - Previous Development ATLAS Beam Steering Mechanism (BSM)

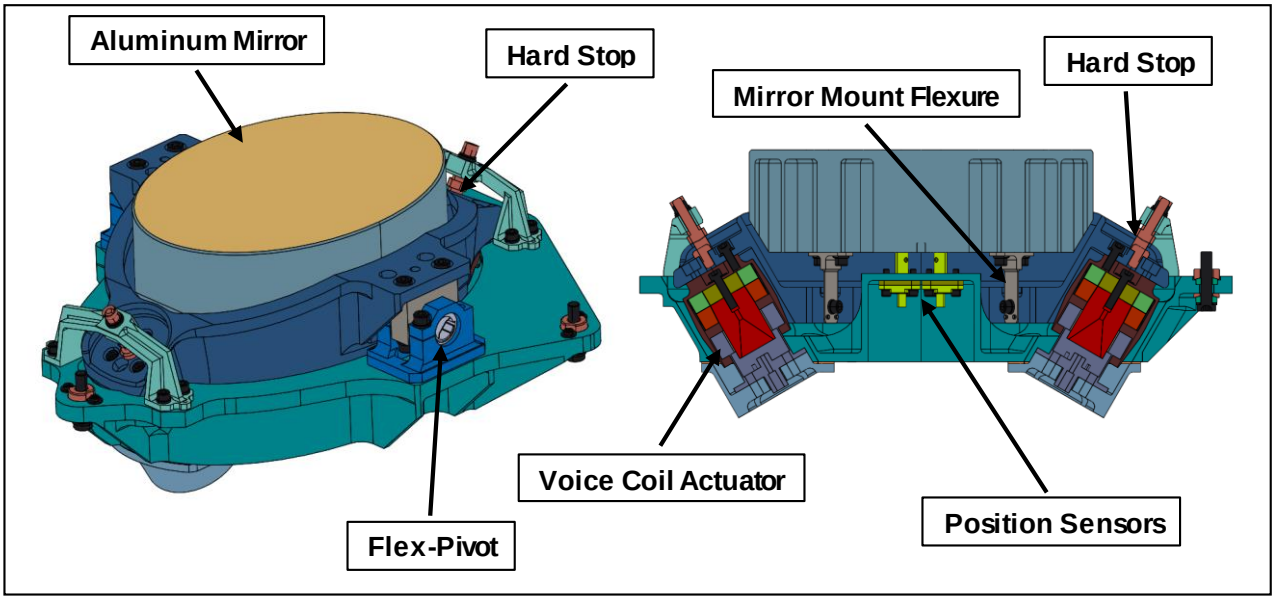

Figure 2 - New Development L'Ralph Scan Mirror Mechanism (SMM)

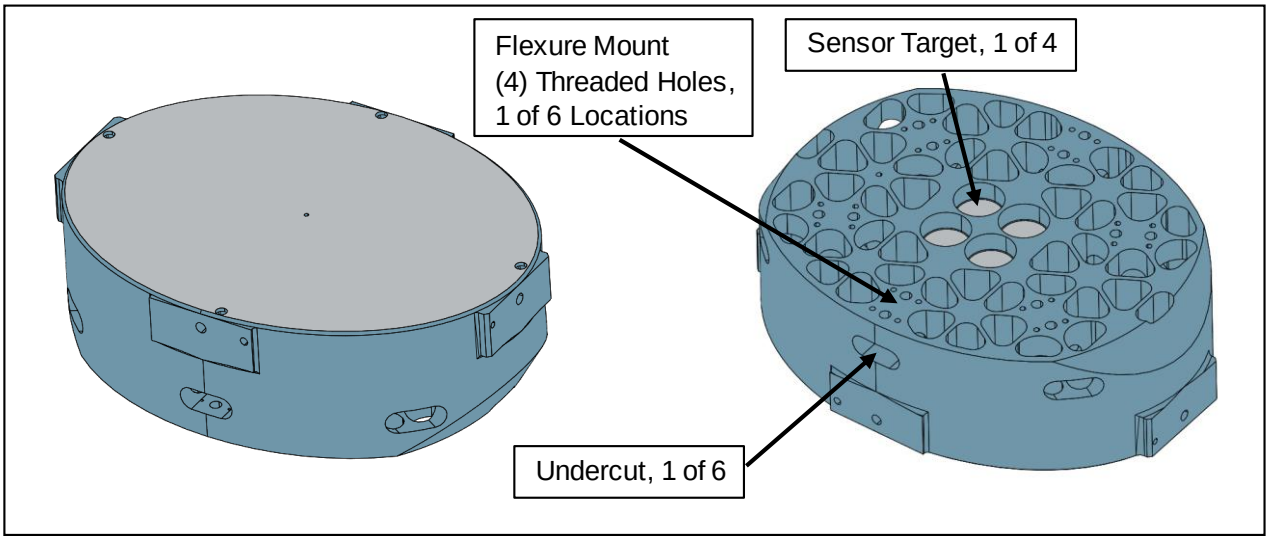

Figure 3 - Lightweighted Aluminum Scan Mirror

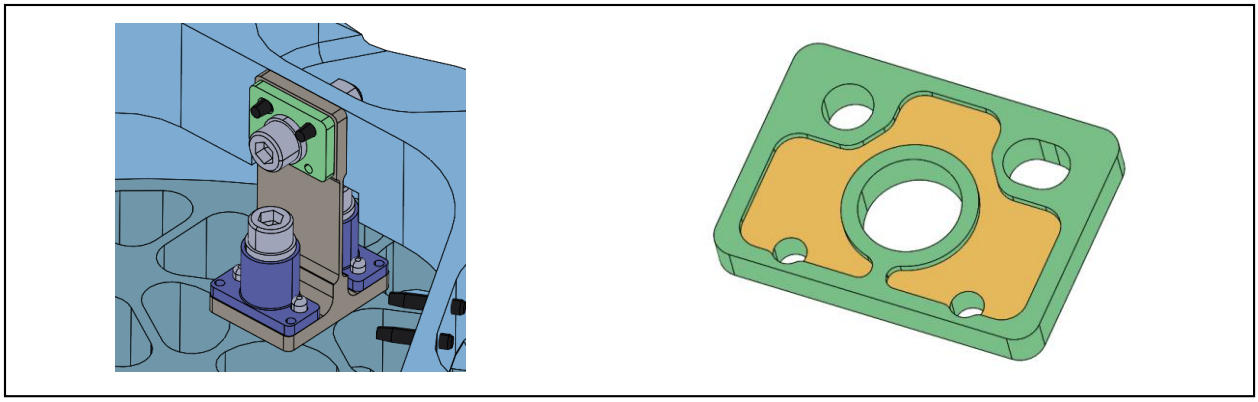

Figure 4 - One of Three Mirror Mount Flexures with Associated Plate for Liquid Pinning

Prototype testing early in the design process uncovered a high sensitivity of mirror flatness to the flexure bolt preload torques. This finding resulted in two significant design changes. The first change was to remove mirror material under the flexure installation locations creating an undercut (Figure 3) such that strains could not propagate to the optical surface directly. This change was effective but did not alone minimize errors to acceptable levels. A second change was implemented to result in lower bolt preload in the cold operating environment while also maintaining preload at ambient conditions to prevent interface gapping under launch vibration. This was achieved using a low-CTE titanium bolt and high-CTE aluminum standoff (Figure 4). Figure 5 provides thermal gradient sensitivity analysis results of the mirror surface. Vibration and low temperature interferometric tests confirmed the soundness of this strategy. Figure 6 provides one of the interferometric test results.

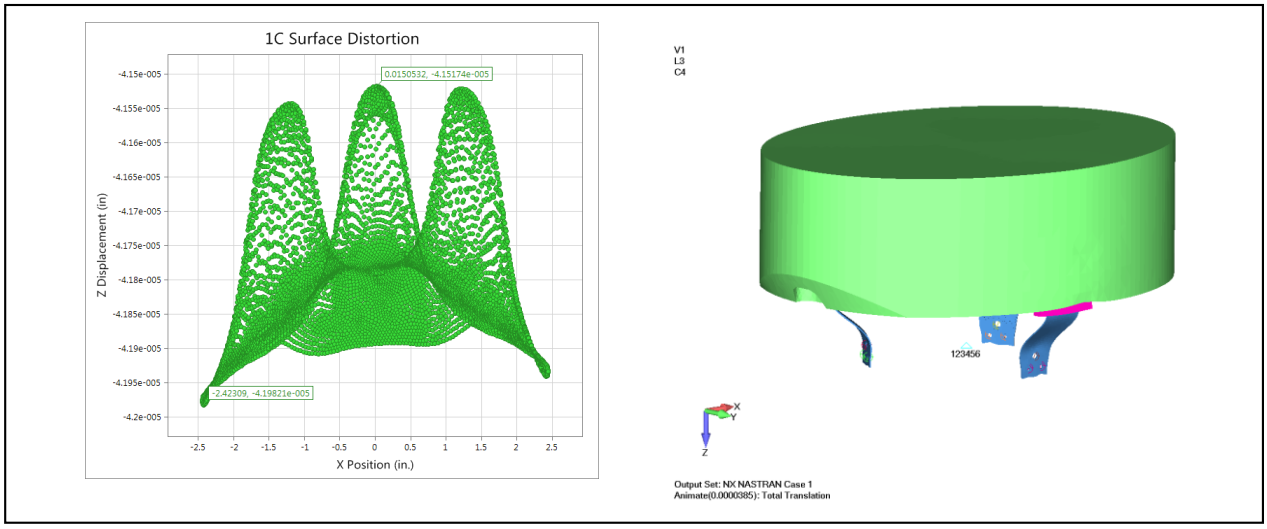

Figure 5 - Thermal Gradient Sensitivity Analysis

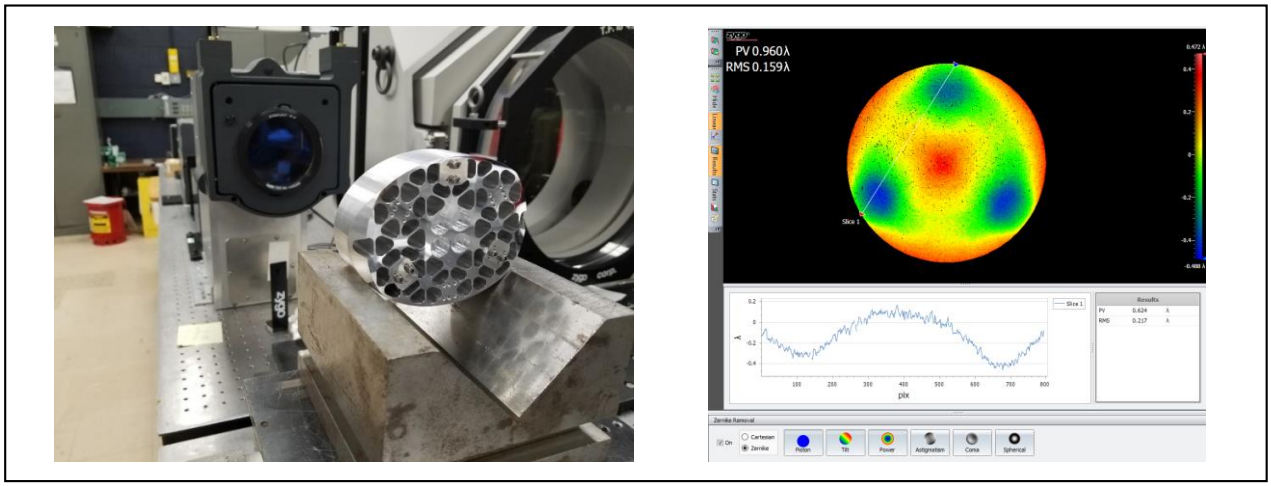

Figure 6 - Prototype Flexure Torque Interferometric Assessment

Strength testing of the aforementioned liquid pin joints was performed to assess shear load capability of the bonds. This testing was critical to the convergence of a design capable of withstanding launch loads. Injection and bond geometry, surface preparation, and adhesive selection were all adjusted as a result of these tests. The first attempt revealed that the injection inlet and outlet size and cavity depth would only allow very low viscosity polymers to flow, limiting selection to materials whose strength was insufficient. Increasing the size of these features also allowed the use of larger injection needles and more manageable injection pressure. Sanded, grit-blasted, and etched/primed surface preparations were evaluated. The grit blasting process proved too aggressive for use with these very small samples, as the cavity containing walls were eroded, allowing adhesive to migrate out of the cavity. There was no significant difference between the sanded and etched/primed samples, however the latter approach was selected for flight (FLT) because the primed surfaces were expected to maintain good surface preparation longer than sanded surfaces. An in-process low temperature interferometric evaluation was performed after the surfaces were prepared but before the cavities were injected, since the stability of the bond surface over time is critical. Flight design and process selection involved coupon testing, depicted in Figure 7.

Figure 7 - Liquid Pin Joint Shear Load Measurement Test Setup and Coupons after Joint Failures

Scan Mirror System (SMS) Performance Verification

The SMM Engineering Test Unit (ETU) vibration tests, which included 22 g sine burst, swept sine, and random, were deemed very successful with no evidence of damage to the structure, no degradation of mirror figure, and no damage to the flex-pivots. Post-test inspections did however suggest that the neutral angle of the mirror had changed slightly with respect to the fixed housing as a result of flex-pivot shift despite being clamped. To correct this issue in the FLT design, alignment and preload-angle clocking features were milled into the flex-pivots to engage with set-screws in the clamps. Non-destructive X-ray cross-section evaluations of the pivots were performed before and after these modifications to ensure that the brazed joints were not disturbed. Figure 8 is an X-ray cross-section of the flex-pivot with the clocking features.

The major challenge of performance verification for this system was to accurately measure commanded mirror position across the on-orbit operational temperature range of -120° C to -89° C. A primary and redundant DPSS is used in L'Ralph to provide mirror position feedback for closed-loop control. Each DPSS was tested by the vendor at various temperatures within the operating temperature range to validate performance, but that testing was performed with a flat double sided aluminum target on the moving portion of a linear stage placed between an opposing differential sensor pair on the fixed portion of that stage. The sensor arrangement in L'Ralph is different, with each sensor of a pair arranged side-by-side and its relatively large angular rotation of +/- 36 mRad might add some non-linearity since the target becomes less orthogonal to each sensor as the mirror moves away from mid-range. Furthermore, each sensor target at the back of the mirror is at the bottom of a counterbore, so there is possibility of a non-linearity contribution by the cylindrical conductive surface surrounding each sensor. Any non-axial motion of the mirror resulting from flex-pivot behavior could be yet another contributor to sensor non-linearity. Therefore, validation of commanded mirror position was a necessity at the mechanism level.

The ATLAS BSM also required mirror position validation while in a thermal vacuum (TVAC) test chamber. The solution was to use an Inter-target Differential Electronic Autocollimator (IDEA) developed by Leviton Metrology Solutions, Inc. This is a very compact optical instrument as compared with a typical autocollimator. One of its features is the ability to measure the mirror angle of interest while calibrating against a reference mirror, which we located on the fixed portion of the mechanism under test. With IDEA looking through a window on the chamber, motion of the mechanism mount within the chamber is calibrated out by the fixed reference measurements. The IDEA system that was custom developed by the vendor for BSM was limited to measuring an angle somewhat beyond that of the BSM range of motion of +/- 5 mRad. A new version of IDEA was developed by the vendor with the capability to measure with some margin beyond that of the L'Ralph angular range of +/- 36 mRad.

The FLT SMM was installed into the TVAC chamber shown in Figure 9. At specific temperature plateaus, whether at qualification or operational, the SMM dwelled for approximately four hours in order to attain sufficient thermal settling of the mechanism. The flex-pivots, provided a constricted thermal path requiring somewhat long dwells to achieve a reasonable temperature gradient that would be good enough for validating mirror angle. Thermal cycle plots at each side of a flex-pivot and mirror are shown in Figure 10.

Controller Performance Change Over Temperature

Controller parameters were initially optimized at ambient temperature resulting in a 30 Hz bandwidth. Frequency response measurements were taken at various TVAC temperatures as shown in Figure 11. It was found that controller performance became less optimal as temperature decreased. As a result of reduction in resistivity of the copper damping sleeve, damping increased with decreasing temperature, ultimately by about a factor of 2.6 going from 25° C to -130° C. Though high damping is very beneficial in terms of disturbance rejection, it was necessary to optimize the controller within the SMM operational temperature range. Thus, controller parameters were chosen to provide optimal performance at operational temperatures. A process of system identification was performed while undergoing TVAC to determine damping as a function of temperature. Fortunately, controller performance, though not optimal at 25° C, was adequate to perform ambient testing without the need to change controller parameters.

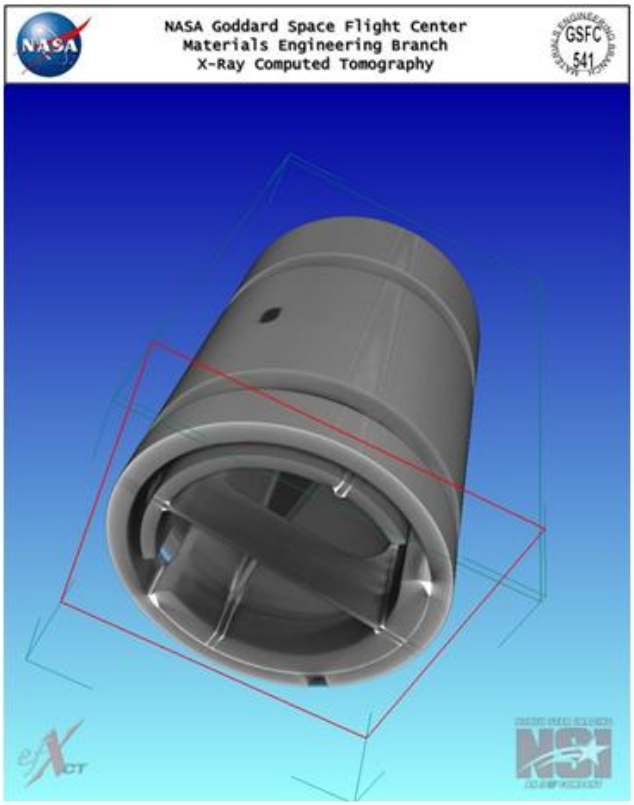

Figure 8 - Flex Pivot X-Ray Cross-Section

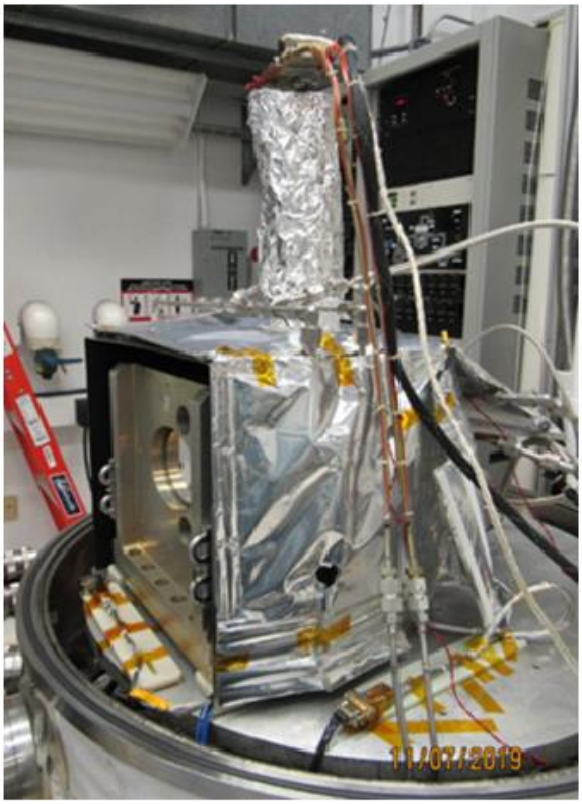

Figure 9 - TVAC Chamber before Closure

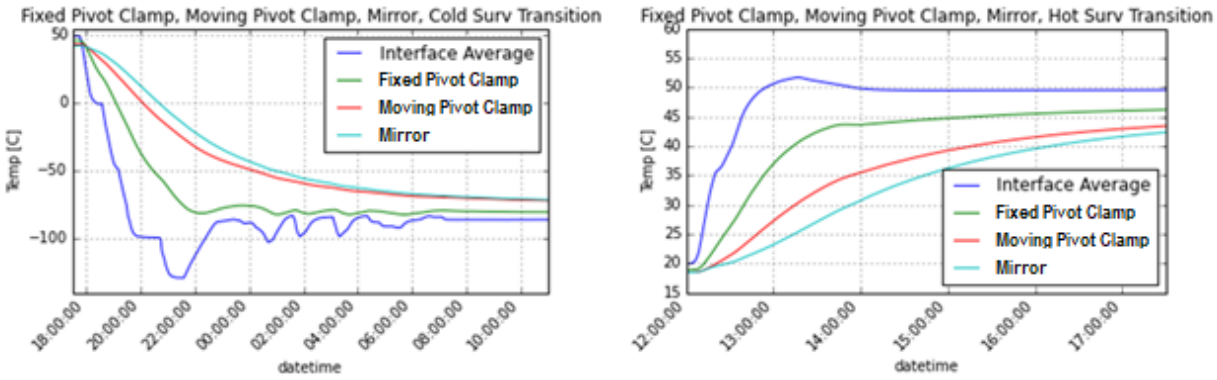

Figure 10 - Fixed Pivot Clamp, Moving Pivot Clamp, and Mirror Temperature Transitions

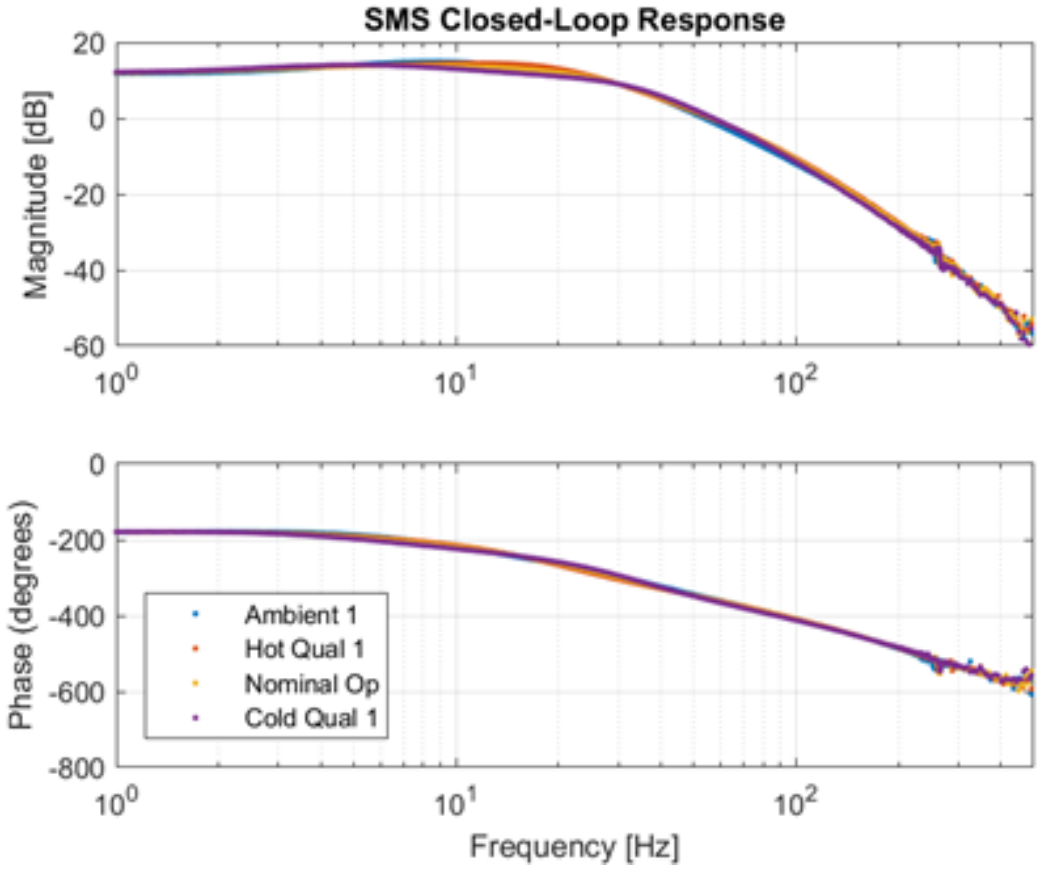

Figure 11 - Closed-loop Bode Plots of the SMS at Various Temperatures

Mirror Position Sensor System Non-Linearity and Thermal Error Correction

Non-Linearity Correction

The original MCE FPGA design had only gain and offset terms for converting DPSS voltage to mirror angle. It was decided to expand this to a third-order polynomial correction to compensate for higher-than-expected non-linearity in the DPSS output. The DPSS tuning process balances non-linearity, thermal stability, and resolution; the latter two were deemed more important to correct in hardware, though non-linearity could be corrected in firmware. At the mechanism level, calibration was performed with our autocollimator as a reference. At the instrument level, calibrations will be performed by scanning across a known star field prior to each encounter. This correction is a polynomial which is computed on each 5 kHz position sample before it is passed to the feedback input of the mechanism's closed-loop controller.

Performance testing at each environment started with sensor recalibration, where static DPSS voltage measurements were compared to autocollimator measurements at over 200 points across the range of motion. The remaining scripted tests were divided into three parts; stability, repeatability, and scan tests. For the stability tests, the SMS was commanded to dwell for several minutes each at various fixed positions across the optical range of the mirror while data such as pointing stability, pointing error, and standby power were captured. Repeatability tests commanded the SMS to a series of test positions in a cyclic manner to ascertain how repeatably the mechanism was able to position the mirror. Finally the SMS was commanded to scan across several optical ranges at several scan rates to obtain data such as optical smear, torque, and scan power. These tests were automated, and test results were trended across the entire mechanism test campaign to verify the performance of the mechanism against system requirements.

Mechanism performance testing showed all requirements were achieved except for one: the pointing resolution requirement. DPSS gain and non-linearity vary with temperature, but because of recalibration prior to each test, there was no noticeable performance degradation across the range of qualification temperatures. The pointing resolution issue appears to be a result of thermal gradients present during the sensor calibration step, which ultimately led to large residuals in the calibration data and thus inaccurate sensor parameters for the controller. To obtain valid calibration parameters, it was necessary wait until mechanism temperature was stable to within ±1.5° C of the desired temperature plateau. As a result, there were consistent pointing errors, especially at the end-of-travel positions where non-linearity is higher, and least-squares polynomial fitting has the highest residuals. Rate and smear are the driving requirements for this mechanism, so relaxation of the pointing resolution specification was deemed acceptable by the project.

Thermal Error Correction

Initial tests of the Engineering Test Unit (ETU) SMS revealed a drift in mirror position with a time constant on the order of 20 seconds. In stability tests where the SMS was commanded to step and hold at a mirror position, the DPSS would report the SMM mirror position as stable at the commanded location, while autocollimator measurements would show the SMM mirror had overshot and was slowly settling into position. The inverse was true in tests where a constant current was used to drive the SMM into one of its hard-stop locations: the autocollimator would show the mirror angle to be static as expected, while DPSS measurements would show the SMM mirror had undershot and was slowly drifting to the expected location. Further testing showed that the initial amplitude of this drift scaled linearly with the size of the step: a larger step meant a larger initial error. Stepping from one end of travel to the other, a 70 mRad motion, led to approximately 200 µRad of initial error.

This drift turned out to be a thermal phenomenon correlated with self-heating of the sensor heads themselves. An experiment was run by the vendor where a single sensor head was heated approximately 1°C, which resulted in a voltage error equivalent to less than 1 mRad, decaying with a similar time constant to what was seen in the SMS. The vendor found by measurement under normal operation, power dissipation of a single sensor head changed by a few milliwatts. Based upon the sensors head's approximate thermal resistance, moving the SMM from one end of travel to the other would lead to a fractional °C change in temperature for a sensor pair. Based on the results of the sensor heating experiment, that temperature delta would cause a voltage error consistent with what was observed in SMS

testing. Further experimentation by the vendor included measuring the temperature change of the sensor heads with thermocouples for full-range moves of their test fixture. Results from this testing show both that full-range steps cause the temperature deltas predicted by the sensor head heating test, and that the time constants of both the temperature change and position error are roughly correlated.

To minimize impact on the existing controller design, correction for this drift was handled within the FPGA firmware but outside the feedback loop. An algorithm that predicted the sensor drift was summed with the position command input.

The results in Figure 12 show a comparison of full-range step response utilizing the correction algorithm to correct for the sensor drift ("Cmd Shaping" in orange) and without it ("No Shaping" in blue). The top plot shows voltage measurements from the DPSS converted to angle, while the bottom shows angle measurements from the autocollimator. When tuned properly, correcting the sensor drift in this way was able to reduce the overshoot error by a factor of 10, from 150 microradians (μRad) down to 15 μRad. TVAC testing has shown that the parameters of this correction vary both with pressure and temperature. Analysis of that data is ongoing.

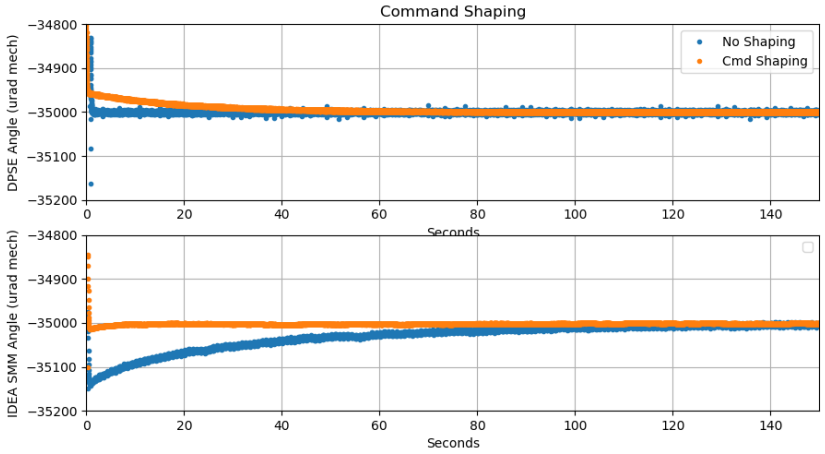

Figure 12 - Command Shaping Performance Improvement

Mechanism Control Electronics (MCE) Development Strategy

Aggressive schedule demands required a compressed MCE development schedule. Three distinct builds were designed: an Engineering Model (EM), an Engineering Test Unit (ETU), and a Flight build (FLT). This design flow allowed early design validation, while providing the necessary hardware for interface and controller development and testing.

The first EM MCE build utilized commercial equivalent parts instead of flight grade parts. Dual footprints were incorporated into the layout to accommodate package differences between flight grade and commercial parts. To prevent schedule delay due to a roughly 1-year EEE part lead time, an alternate (but functionally identical) part was used for the power op-amp. A reprogrammable FPGA module was used for development in place of the one-time-programmable FPGA that would be used on the FLT boards. A build plan change added two EM MCE boards to facilitate controller testing and development, and interface testing. This also meant the schematic and Printed Circuit Board (PCB) layout were verified before ETU/FLT

and allowed for a dry run of the assembly process. Board level electrical checkout and functional testing procedures were also developed at this stage. A minor net-swap issue was found in the schematic design and fixed with a white wire on the EM, and the schematic and layout were updated for FLT PCBs.

Since the SMM was not available early enough for initial EM board testing, a mechanism simulator was built. The structure was 3-D printed, and commercial flex-pivots and a prototype aluminum mirror were used to closely match the expected plant dynamics. Commercial voice coil actuators and a commercial DPSS allowed open-loop and closed-loop testing. This rapid prototype allowed controller and FPGA development to move forward months before the ETU SMM would be available. It was also useful as a stand in for the ETU SMM and invaluable for testing the optical verification setup. Views of the mechanism simulator are shown in Figure 13.

The ETU builds utilized parts appropriate for environmental testing. The second ETU build was assembled with the updated FLT PCB. By working out assembly and test procedures on the EM and ETU builds, it was possible for FLT assembly and test to be completed very rapidly. Because the FLT FPGAs are not reprogrammable, a FLT FPGA was burned and installed on an EM board first to verify the design was successful, buying down risk. The FLT MCE is shown in Figure 14.

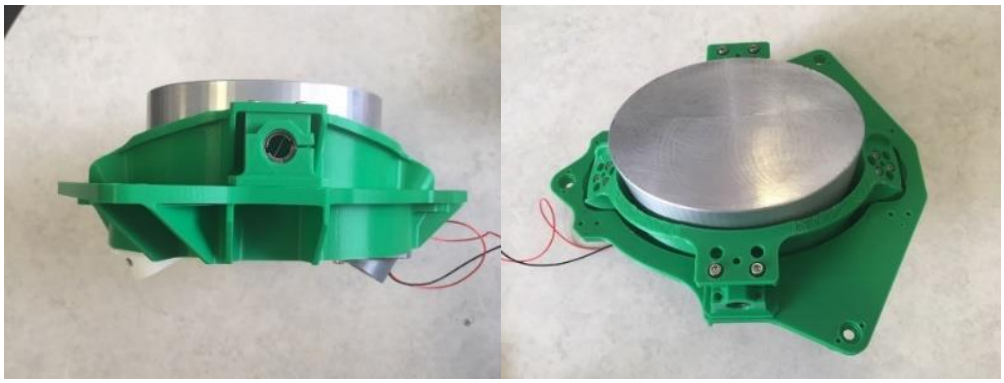

Figure 13 - Mechanism Simulator

Figure 14 - L'Ralph Flight Mechanism Control Electronics (MCE)

Flexibility of the Controller Was Crucial to Project Success

As previously discussed, the digital FPGA-based controller allowed for correction of position sensor system non-linearity and thermal error. It also facilitated system identification at low temperature to determine damping by allowing adjustment of controller parameters. However, at the start of the project, a digital controller was not the baseline.

During the proposal phase, an analog controller with a simplistic digital section was chosen as the baseline. One reason for that selection was that a digital controller utilizing an FPGA was deemed too power hungry to meet the power constraints for this mission. Power had been originally determined using values from an FPGA-based digital controller used on another project. A second reason is that a grassroots cost estimate resulted in a significantly lower cost for the analog design over the FPGA design. Once the project was awarded, the product design lead, the primary author of this paper, had tremendous concern about lack of flexibility and resulting excessive risk of the baselined MCE approach. While there were perceived benefits in terms of power and cost for the baseline choice, subsequent analysis found that power could be met with an FPGA-based design, and further review found that manpower beyond what was baselined would be required to develop the seemingly simple discrete electronics. The project ultimately agreed to change the plan and develop an FPGA-based MCE.

As a lesson learned, it became apparent near the end of this project how important this decision was. If the MCE was not FPGA-based, it would have lacked the flexibility to correct position sensor issues as well as assist with system identification when in TVAC. Without the FPGA-based MCE, some crucial specifications would not have been met thus negatively impacting the science.

As a rule, it is of critical importance that the design architecture be correct from the beginning. With today's schedule and budget constraints, it is very difficult to change course when problems arise. Thus, diligence must be exercised to get it right the first time because there is typically not time for an additional iteration. Sound arguments and perseverance are necessary ingredients to gain project approval if it becomes necessary to change the path forward to that with the lowest practical risk.

Conclusion

The L'Ralph SMS team had the benefit of leveraging the previous ATLAS BSM development. The SMS at first was thought to be a straightforward task since compared to the BSM, it appeared to be less challenging. The SMS would be a single axis system rather than a dual axis system, utilize off-the-shelf flex-pivots rather than require development of a custom flexure, would have a similar DPSS and a similar MCE, and was specified to have about seven times coarser resolution than the BSM. Yet, the requirements were quite different resulting in an SMM that looks very different from the BSM, and a new set of development challenges came about. The team was highly motivated, enjoyed the challenges, and gained a new set of lessons learned that we are sharing with the aerospace mechanisms community via this paper. The team can be proud of the SMM final product, which supports an incredible mission that will advance our knowledge of planet formation. Figure 15 and Figure 16 are views of the FLT SMM.

Acknowledgements

Michael G. Edick***, Theodore J. Hadjimichael*, William M. Hansell**, Douglas B. Leviton****, David W. McClaeb*, Joseph C. McMann*****, Armando Morell**, Matthew A. Owens***, Gary L. Sheridan**, and Patrick L. Thompson*.

* NASA Goddard Space Flight Center, Greenbelt, MD

** ATA Aerospace, LLC, Greenbelt, MD

*** Florez Engineering, LLC, Laurel, MD

**** Leviton Metrology Solutions, Inc., Boulder, CO

***** Orbital Sciences Corp., Greenbelt, MD

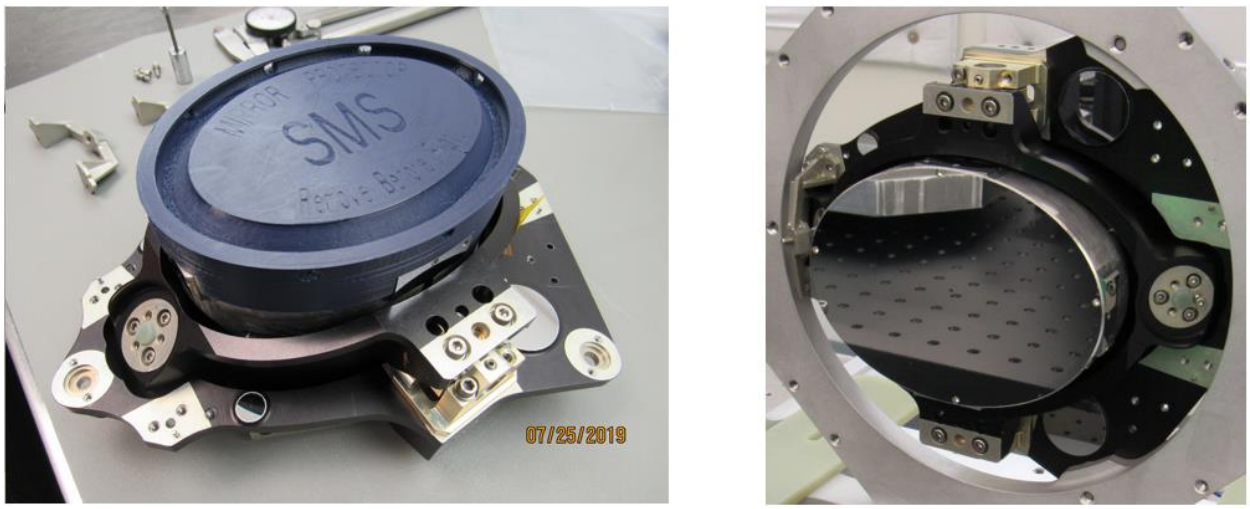

Figure 15 - L'Ralph FLT Scan Mirror Mechanism (SMM) Mirror View

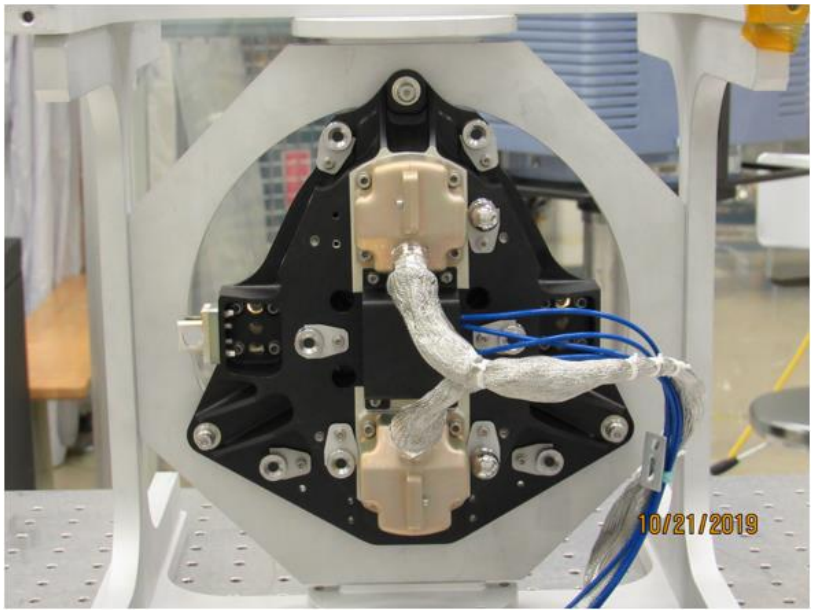

Figure 16 - L'Ralph FLT Scan Mirror Mechanism (SMM) Rear View

References

1. Blumenstock, Kenneth A., et al. "ATLAS Beam Steering Mechanism Lessons Learned." *Proceedings of the 43rd Aerospace Mechanisms Symposium*, (May 2016), pp. 1-14.
2. Donegan, Richard J. "Weld versus Braze." [Engineering considerations regarding electron beam welded versus brazed flex-pivots]. *Retrieved from* http://riverhawk.com/weld-versus-braze/, (n.d.)